1

The effect of sample drying temperature on marine particulate organic carbon composition

Sarah Z. Rosengard[1,2*], Phoebe J. Lam[3], Ann P. McNichol[4,5], Carl G. Johnson[2], Valier V. Galy[2]

1. Massachusetts Institute of Technology Department of Earth, Atmospheric and Planetary Sciences, Cambridge, MA, U.S.A.
2. Woods Hole Oceanographic Institution Department of Marine Chemistry and Geochemistry, Woods Hole, MA, U.S.A.
3. University of California-Santa Cruz Department of Ocean Sciences, Santa Cruz, CA, U.S.A.
4. Woods Hole Oceanographic Institution Department of Marine Geology and Geophysics, Woods Hole, MA, U.S.A.
5. National Ocean Sciences Accelerator Mass Spectrometry Facility, Woods Hole, MA, U.S.A.

Corresponding author contact: (tel) 646-361-1195; srosengard@eoas.ubc.ca
* current affiliation: University of British Columbia Departments of Geography and Earth, Ocean and Atmospheric Sciences, Vancouver, BC, Canada

Abstract

Compositional changes in marine particulate organic carbon (POC) throughout the water column trace important processes that underlie the biological pump's efficiency. While labor-intensive, particle sampling efforts offer potential to expand the empirical POC archive at different stages in the water column, provided that organic composition is sufficiently preserved between sampling and analysis. The standard procedure for preserving organic matter composition in marine samples is to immediately store particles at -80°C to -20°C until they can be freeze-dried for analysis. This report investigates the effect of warmer drying and storage temperatures on POC composition, which applies to the majority of POC samples collected in the field without intention for organic analysis. Particle samples collected off Woods Hole, MA were immediately dried at 56°C, at room temperature, or stored at -80°C until being freeze-dried. Results show that oven- and air-drying did not shift the bulk composition (i.e., carbon and nitrogen content and stable isotope composition) of POC in the samples relative to freeze-drying. Similarly, warmer drying temperatures did not affect POC thermal stability, as inferred by ramped pyrolysis/oxidation (RPO), a growing technique that uses a continuous temperature ramp to differentiate components of organic carbon by their decomposition temperature. Oven- and air-drying did depress lipid abundances relative to freeze-drying, the extent of which depended on compound size and structure. The data suggest that field samples dried at room temperatures and 56°C are appropriate for assessing bulk POC composition and thermal stability, but physical mechanisms such as molecular volatilization bias their lipid composition.

1   Introduction

Marine particulate organic carbon (POC) is the primary vector for the biological pump, which transfers ~0.2 Gt carbon/year - approximately 0.1 % marine primary productivity - to the seafloor (Burdige 2007). These particles harbor thousands of distinct organic biomolecules generated predominantly by primary producers and heterotrophs (Repeta 2014). Changes in this biomolecular matrix in the water column reflect important processes that govern the transport and recycling of marine POC (Burd et al. 2016). Techniques for describing changes in this matrix range from measuring bulk characteristics that are an integration of all biomolecules (e.g., the stable isotope composition of total POC, reported as $\delta^{13}C$) to quantifying smaller abundances of specific biomolecules (e.g., the abundance of lipid biomarkers and their $\delta^{13}C$ values) (Wakeham and Volkman 1991; Trull and Armand 2001; Cavagna et al. 2013).

To accurately interpret the composition of POC in the water column, its organic matrix must be preserved between collection and analysis. Prior studies have demonstrated a link between wet sample storage temperature and organic matter preservation. For example, storage at room temperature can promote microbial degradation in the sample matrix, significantly altering the distribution of lipid abundances after one month (Grimalt et al. 1988). But, even longer term storage at temperatures below freezing can alter the lipid composition of organic matter by rupturing cell membranes and concentrating enzymes in solution, increasing the extraction efficiency of free fatty acids and preferentially breaking down polar lipids (Wakeham and Volkman 1991; Ohman 1996). Current recommendations are that marine

71 samples intended for organic analysis are frozen immediately after collection and stored

72 at -80°C to -20°C and freeze-dried prior to analysis, which minimizes alteration of

73 organic matter composition by heterotrophic remineralization after sampling (Wakeham

74 and Volkman 1991).

75   Still, the majority of particulate matter collected at sea is not intended for organic

76 analysis. Samples for bulk elemental analysis are often dried in a heated oven, and

77 samples for inorganic analysis are sometimes air-dried, and then stored at room

78 temperature before analysis (e.g., Buesseler et al. 2005; Bishop and Wood 2008; Bishop

79 et al. 2012; Lam et al. 2015; Rosengard et al. 2015), rather than being freeze-dried. The

80 tremendous labor, financial cost and scientific potential of sampling marine particles

81 warrants an investigation into how much POC integrity is sacrificed when different

82 sample drying methods do not meet optimal standards of organic geochemical analysis

83 (Wakeham and Volkman 1991). This paper compares the effects of freeze-drying

84 samples, air-drying samples at room temperature, and oven-drying samples at elevated

85 temperatures on three aspects of organic composition: bulk organic matter composition

86 (C/N ratio, $\delta^{13}C$ and total organic carbon content), biomolecular composition (specific

87 lipid abundances), and thermal stability.

88   In this report, the latter metric for composition, thermal stability, refers to the

89 distribution of temperatures over which a POC sample decomposes to CO_2 during

90 ramped pyrolysis/oxidation (RPO), a novel but increasingly utilized technique for

91 characterizing the composition of organic matter in the environment. By pyrolyzing or

92 oxidizing POC throughout a controlled temperature ramp from ~100°C to 800°C, and

93 monitoring the release of CO_2 throughout the ramp, this technique differentiates distinct

4

94 pools of bulk organic carbon by their thermal stability, reflecting the activation energy of

95 decomposition/oxidation of specific POC pools in the sample (Cramer 2004). RPO has

96 been applied over a range of organic matter samples from complex depositional

97 environments, from suspended riverine POC to ocean sediments (Rosenheim et al. 2008;

98 Rosenheim and Galy 2012; Rosenheim et al. 2013; Subt et al. 2016). Thus, RPO of

99 marine POC offers a unique opportunity to relate POC composition to its biological

100 reactivity in the environment, which impacts the strength of the biological pump

101 (Francois et al. 2002; Burd et al. 2016).

102   We hypothesized that air-drying and oven-drying a sample would negligibly

103 influence the bulk composition and thermal stability of POC (e.g., Kaehler and

104 Pakhomov 2001). The energy imposed by high-flow air-drying and oven-drying relative

105 to freeze-drying is too small to shift the bonding energies (Wagner et al. 1994) and

106 therefore the activation energies of thermal decomposition in the biomolecular matrix

107 (Cramer 2004). Moreover, these approaches dry particle samples within 24 hours, which

108 likely minimizes microbial degradation of POC in the sample. By contrast, we expected

109 air-drying and oven-drying to shift the absolute and relative abundances of specific

110 biomolecules in POC, which are typically present in trace quantities. Indeed, Wang et al.

111 (2017) observed that lipid distributions in soils shifted in response to heating at

112 temperatures as low as 60°C. The results of these comparisons have several implications

113 towards the opportunistic use of marine particle samples for organic analysis, even when

114 not processed according to ideal organic geochemical standards.

115

2   Materials and procedures

Different drying treatments were compared using samples of marine POC collected off the dock of the Woods Hole Oceanographic Institution (WHOI), at 41.524°N, 70.672°W, in June 2014.

2.1   Sample collection

To collect marine particles, a battery operated *in situ* pump (McLane WTS-LV) was deployed ~10 meters below surface and pumped seawater through two identical flow paths (Lam et al. 2015). Each flow path directed seawater through a 51 µm pore-size polyester pre-filter screen followed by a pair of pre-combusted 1 µm pore-size quartz fiber filters (Whatman™ quartz membrane grade A, or QMA), both mounted onto "mini-MULVFS" filter holders (Bishop et al. 2012). The active collection area of these filters was 125 cm^2. The pre-filter retained >51 µm size-fraction particles, while the QMAs collected 1-51 µm size-fraction particles, most of which settled on the first QMA filter of the flow path. After ~45 minutes, or 40-100 L seawater filtered, the filters clogged and the pump stopped.

The pump was deployed twice, collecting two pre-filters and two pairs of sample QMA filters (POC1 and POC2) over both flow paths in the first deployment, and one pre-filter and one pair of QMA filters (POC3) from one flow path in the second deployment (Table 1). During each deployment, a deployment blank sample was also collected by submerging a complete filter set - a 51 µm pre-filter and a pair of QMA filters -

139   sandwiched between 1 µm mesh filters to exclude particles, in a perforated plastic

140   Tupperware box, which was externally attached to the McLane pump frame. The second

141   pump deployment immediately followed the first. Depth control was poor, so the two

142   deployments likely occurred at slightly different depths.

143   Of all filters deployed, only the QMA filters, which collected <51 µm particles,

144   were analyzed. Of the three pairs of particle filters collected, only the topmost QMA filter

145   relative to the pump's flow path was analyzed, as this filter likely retained most <51 µm

146   particles (Fig. 1a, c). For each pair of the two deployment blank filters, we considered

147   differences between the two QMA filters to be negligible (Fig. 1b). Each sample and

148   deployment blank filter was divided into thirds prior to drying, such that each drying

149   treatment could be applied in triplicate. As Section 3 argues, this dividing scheme helped

150   account for environmental heterogeneity associated with particle sampling in POC-rich

151   waters during analysis of thermal and lipid composition of the samples (Sections 2.3-2.4).

152   One third was immediately frozen at ~-10°C, transferred to -80°C two weeks later, and

153   finally freeze-dried overnight before analysis (Fig. 1, Table 1). Another third was placed

154   in an oven for drying at 56°C for 17-19 hours. Finally, one third was dried under a clean

155   laminar flow hood at high air flow and room temperature for 17-19 hours. All oven-dried

156   and air-dried filters were stored in Whirl-Pak bags or combusted glassware at room

157   temperature before analysis. All analyses were done within one year of sample collection.

158   Prior to analysis, images of dried QMA filters were developed at various

159   magnifications for a freeze-dried portion of deployment blank and sample filters using a

160   scanning electron microscope (SEM) (Fig. 1b, c). No coccoliths or other calcium

161   carbonate shells were observed in the sample filter. Thus, we assumed that the particulate

162 inorganic carbon content (PIC) in the particle samples was negligible, and would not

163 interfere with any of the POC analyses described in the following sections. The stable

164 isotope data reported in the "Assessment" section will address this assumption.

165

166 **2.2   Bulk composition analysis**

167

168   The bulk composition (particulate organic carbon concentration ([POC]),

169 particulate nitrogen concentration ([PN]), $\delta^{13}C$ and $\delta^{15}N$) of the dried QMA filters was

170 analyzed using a *Fisons Instruments Carlo / Erba 1108* elemental analyzer interfaced via

171 a *Finnigan MAT Conflo II* to a *Thermo Finnigan Delta-Plus* stable isotope ratio mass

172 spectrometer. These analyses were intended to guide our choice of filter sub-sample size

173 for ramped pyrolysis/oxidation (RPO) analysis, while maximizing the amount of sample

174 left for RPO and lipid analysis (Section 2.3). Thus, for each drying treatment, only ~0.9%

175 of the active area of a whole QMA filter (125 cm^2) from a different filter replicate was

176 analyzed in bulk: the freeze-dried sub-sample of particle filter POC2, the air-dried sub-

177 sample of filter POC3, and the oven-dried sample of filter POC1 (Table 1). One

178 deployment blank sub-sample (~0.9% QMA active area) from a freeze-dried filter portion

179 was analyzed, as well.

180

181 **2.3   Ramped oxidation analyses**

182

183   The ramped pyrolysis/oxidation (RPO) system at the National Ocean Sciences

184 Accelerator Mass Spectrometry (NOSAMS) facility converts sample organic carbon to

8

185   carbon dioxide (CO_2) gas through a continuous temperature ramp, either by pyrolysis or

186   oxidation, depending on the instrument plumbing (Hemingway et al. 2017). For each

187   drying treatment, the same size subsamples across the particle sample or deployment

188   blank replicate filters were combined prior to analysis, equating to 3-5% of the active

189   sample filter area or ~9% of the deployment blank filter area. Particle sub-samples were

190   analyzed three times, resulting in three thermograms per drying treatment that recorded

191   CO_2 evolved during the temperature ramp (Fig. 2a-c). Deployment blank filters were only

192   analyzed once. Furthermore, ~5% of a pre-baked (up to 450°C) but non-deployed QMA

193   filter was also analyzed by ramped oxidation.

194   All RPO analyses were conducted following protocol described in Rosenheim et

195   al. (2008) and Hemingway et al. (2017). All filter subsamples were inserted into a quartz

196   reactor inside one of two furnaces (referred to as ovens A and B) programmed to heat at

197   5°C/minute from room temperature to 1000°C (Table 2). During the temperature ramp,

198   roughly 35 mL/min of ~92% Ultra-High Purity helium and ~8% oxygen gas flowed

199   through the quartz insert from the programmed furnace, carrying oxidation products to an

200   800°C furnace equipped with a copper, platinum and nickel catalyst that fully converts

201   the products into CO_2 gas. Consistent flow rates, $He:O_2$ proportions in the gas source,

202   furnace catalyst and insulation, and plumbing across RPO analyses minimized

203   instrumental variation within the data set. Downstream of the catalyst, the CO_2 and

204   carrier gas passed through a *Sable Systems© CA-10* infrared gas analyzer, which

205   measured the outgoing CO_2 concentration, which was calibrated at 0 ppm and >400 ppm.

206   After the gas analyzer, the gas mixture flowed into a cryogenic Pyrex coil that was

207   coupled to a vacuum line, where the CO_2 gas was cryogenically trapped and released into

208 a vacuum line within user-specified temperature intervals. The gas was quantified

209 barometrically and converted to mass to calculate a carbon yield for the entire analysis.

210

211 **2.4   Compound-specific measurements**

212

213   Compound-specific abundances offer the highest resolution comparisons of

214 organic matter composition across drying treatments in this report. We limited analysis to

215 the abundances of fatty acids, sterols and alcohols, which are commonly applied to study

216 marine POC dynamics in the water column (e.g., Wakeham and Canuel 1988; Cavagna et

217 al. 2013).

218   Roughly 5% of the 125 cm^2 sample QMA filter active area and ~7-15% of the

219 deployment blank filter area were extracted in 15-20 mL of 9:1 dichloromethane:

220 methanol (DCM: MeOH) at 100°C for 20 minutes using a *CEMS* Corporation Microwave

221 Accelerated Reaction System. For each drying treatment, the extracts represented the

222 combined, equal sub-fractions of the three sample filters or the two blank filters collected

223 (Fig. 1). After extraction, the total lipid extract was saponified in 0.5 M potassium

224 hydroxide in MeOH for two hours at 70°C. Following saponification, liquid-liquid

225 extractions separated the basic phase from the acidic phase, each of which was eluted

226 through aminopropyl silica gel columns to separate compounds into five compound

227 classes based on their polarity. Fatty acids of both acid and base phases were recombined

228 and methylated for 12 hours at 70°C, and purified through another silica gel column prior

229 to analysis on a flame ionization detector coupled to a *Hewlett Packard 5890 Series II*

230 Gas Chromatograph (GC-FID). Sterols and alcohols of acid and base fractions were

10

231   acetylated separately in acetic anhydride and pyridine (1:1) for 2 hours at 70°C prior to

232   analysis on the GC-FID.

233   All sample and deployment blank analyses were accompanied by quantification of

234   synthetic standards that contained a suite of fatty acids, sterols and alcohols with known

235   concentrations and retention times. Retention times were used to identify specific

236   compounds in the samples and deployment blanks. Other compound identities,

237   particularly those of the unsaturated and branched FAMES, and gorgosterol, were

238   separately validated using an *Agilent 7890A* gas chromatograph interfaced with a

239   *Markes/Almsco BenchTOF-Select* time of flight mass spectrometer. To evaluate sample

240   drying effects on compound abundances, we directly compared peak areas across samples

241   and blanks after normalizing the areas to the fraction of QMA filter active area extracted.

242   Normalized peak abundances errors were assumed to be ~10% based on normalized peak

243   abundances from replicate analyses of the fatty acid standard. Individual peak abundance

244   errors were propagated in all subsequent analyses discussed in Section 3.3.

245

246   **3**   **Assessment**

247

248   The following compares the bulk, compound-specific and thermal composition of

249   marine POC collected from the coastal waters of Woods Hole, MA and treated by oven-

250   drying, air-drying or freeze-drying. To interpret thermal stability, we assume that

251   biomolecules in an organic matrix span a range of activation energies of decomposition

252   (Cramer 2004; Rosenheim et al. 2008; Rosenheim and Galy 2012; Rosenheim et al.

253   2013), which would drive differences in the oxidation temperature of compounds and

254   fragments of compounds during ramped oxidation. Our interpretations of bulk carbon

255   composition and thermal stability rely on the assumption that PIC concentrations in

256   particulate matter are negligible, and that the carbon quantities reported correspond

257   predominantly to organic carbon in the samples. The consistently depleted isotope

258   composition of the bulk carbon corroborates this assumption (Table 1). This is further

259   reflected by the lack of any significant calcifying organisms observed on SEM images of

260   particle sample QMA filters (Fig. 1c).

261

262   **3.1   Invariant bulk composition across drying treatments**

263

264   All carbon and nitrogen quantities measured on three sample QMA filters (one

265   per drying treatment) and one deployment blank filter (freeze-dried only) were

266   normalized to the total active area of the filter (125 cm^2) and volume filtered, yielding

267   total C and N filter loadings and concentrations, respectively (Table 1). Particle sample C

268   loadings ranged from 10.5 - 13.2 mg C/QMA, corresponding to 11.9 - 16.7 µM C. Total

269   N concentrations ranged from 1.8 - 2.5 µM. Because the bulk measurements were

270   conducted on individual filter samples (Section 2.2), variability between McLane pump

271   deployments and environmental heterogeneity of the particle pool drive the range in the

272   total carbon and nitrogen loadings on the QMA filters, in addition to any effects imposed

273   by the different drying treatments.

274   More importantly, despite these differences in the carbon loading among the

275   particle sample filters, relatively invariant bulk δ^{13}C, δ^{15}N and C/N values across filters

276   from different treatments and deployments imply that air-drying and oven-drying do not

277   appreciably affect bulk POC composition relative to freeze-drying (Table 1). Bulk δ^{13}C

278   values of sample carbon ranged from -23.9 ‰ to -23.6 ‰, δ^{15}N values ranged from 7.9‰

279   to 8.3 ‰, and C/N values ranged from 6.5 - 6.8. The standard deviation of the three δ^{13}C

280   (±0.1 ‰), δ^{15}N (±0.2 ‰) and C/N (±0.2 μmol/μmol) values measured across sample

281   filters are comparable to or smaller than the analytical precision of each measurement.

282   The total carbon and nitrogen loadings on the freeze-dried deployment blank filter

283   sub-sample were 10-20 times lower than the bulk content on the three particle sample

284   filters analyzed (Table 1). The δ^{13}C of the blank carbon was -25.6 ‰, ~2 ‰ more

285   depleted than the δ^{13}C values of the particle samples. At the same time, the scanning

286   electron images of the deployment blank filters showed no evidence of particles on the

287   filter fibers (Fig. 1b), consistent with the assumption that the small quantity of carbon on

288   the deployment blank filters is likely sorbed dissolved organic carbon.

289

290   **3.2   Thermal stability not affected by drying treatments**

291

292   All <51 μm combined particle samples and deployment blanks, oven-dried, air-

293   dried and freeze-dried, were analyzed by ramped oxidation between 100°C and 1000°C,

294   with most sample and blank carbon oxidizing between 150°C and 600°C (Fig. 2). In

295   general, the total CO_2 gas evolved during ramped oxidation of each combined particle

296   sample and blank, barometrically quantified in the vacuum line and normalized to the 125

297   cm^2 active area of a QMA filter, served as an estimate of the total sample carbon

298   integrated across all different filter deployments treated by the same drying process

299 (Table 2). The exception was the second freeze-dried sample run, for which no CO_2

300 pressure was quantified and converted to a total carbon yield.

301   The deployment blank RPO analyses provide further evidence for organic carbon

302 sorption onto QMA filters. Thermograms of combined deployment blanks yielded 0.5 -

303 1.1 mg carbon/filter across drying treatments (Table 2, Fig. 2d), 3-10 times greater than

304 the carbon yielded from a pre-combusted unused blank QMA (Fig. 2e), and several

305 orders of magnitude higher than the estimated blank contribution for the NOSAMS RPO

306 system (Hemingway et al. 2017). Carbon yields from the deployment blank analyses

307 were not significantly different across drying treatments, considering that replicate

308 ramped oxidation analyses of the same size sub-sample can vary by as much as 0.07 mg

309 carbon, which exceeds differences among the relatively small carbon quantities yielded

310 during the three deployment blank analyses, pre-normalization (Table 2). Because the

311 amount of carbon on the deployment blank filters represents <10% of the total carbon

312 yield from the combined particle sample RPO analyses, and did not vary significantly

313 among drying treatments, it was not necessary to apply a blank subtraction to the particle

314 sample thermograms in this study.

315   Compared to the bulk analyses, the RPO carbon yields from the combined particle

316 sample analyses represent the average of three deployed filter samples or two deployed

317 blank replicates, and thus remove the influence of environmental heterogeneity

318 associated with different pump deployments and uneven particle loading. Differences in

319 filter area-normalized carbon yields across drying treatments are comparable to the

320 differences among replicate RPO analyses of the same sample, indicating that oven-

321 drying and air-drying do not influence the total carbon loaded on the filters relative to

322 freeze-drying (Table 2; Fig. 2a-c).

323   Similarly, the differences in thermogram shape of combined particle samples

324 across drying treatments are comparable to and do not exceed the differences among

325 triplicate thermograms of samples with the same drying treatment (Fig. 2a-c), suggesting

326 that air-drying and oven-drying do not significantly change the thermal stability of the

327 POC relative to freeze-drying. Use of different programmable ovens could account for

328 some of the smaller differences among the thermogram shapes across triplicate ramped

329 oxidation analyses of the same sample, particularly for the shifts along the temperature

330 axis. Thermograms of replicate sample analyses using the same oven, Oven A (Fig. 2f),

331 line up better in temperature space than repeated analyses of the same sample using two

332 different ovens, Ovens A and B (Figs. 2a-c). In the future, periodically running standard

333 compounds with well-defined peaks, such as sodium bicarbonate, in the different sample

334 ovens would help normalize these temperature shifts in thermograms generated by

335 different ovens (Rosenheim et al. 2008).

336

337 **3.3   Drying temperature alters lipid composition**

338

339   Abundances of fatty acids, sterols and alcohols in combined particle samples and

340 deployment blanks were quantified across a range of molecular sizes. Peaks from each

341 particle sample and deployment blank chromatogram represented an average of the

342 different replicate filters deployed (Section 2.4). The areas of select compound peaks

343 were normalized to the area of an entire QMA filter (Table S1). Next, for each drying

15

344   treatment, filter-normalized peak areas across the deployment blank chromatograms were

345   subtracted from matching filter-normalized peak areas in the sample chromatograms.

346   Finally, we compared ratios of each normalized and blank-corrected peak area in the

347   oven-dried ("O") and air-dried ("A") combined particle samples to corresponding

348   normalized and blank-corrected peak areas in the freeze-dried sample ("F"). For the rest

349   of the discussion, these ratios are $R_{O/F}$ and $R_{A/F}$, respectively. Ratios less than one

350   indicate depression of compound abundances in oven-dried or air-dried samples relative

351   to compound abundances in freeze-dried samples.

352   Unlike the bulk and ramped oxidation data, the lipid analyses imply that oven-

353   and air-drying affected compounds associated with the deployment blank filters

354   differently than they affected the same compounds in the particulate carbon pool. Indeed,

355   for most compounds, $R_{O/F}$ and $R_{A/F}$ ratios in deployment blanks deviated from

356   corresponding ratios in the combined particle samples (Figs. 3c, 4c, 5c; Table S1). For

357   this reason, we applied a blank correction to particle sample abundances to better control

358   for differences between drying effects on the sorbed lipid pool and drying effects on

359   particulate lipid pool. The processes decoupling the sorbed lipid pool from the

360   particulate lipid pool, unlikely to result from methodological errors in sample preparation

361   or contamination of the deployment blank filters, are beyond the scope of this study.

362   Fatty acid analysis spanned a range of molecular sizes, including saturated

363   straight-chain fatty acids (12 to 24 carbon chain lengths, or C_{12}-C_{24}), straight-chain

364   unsaturated fatty acids (C_{14}-C_{22}), and saturated branched fatty acids produced by bacteria

365   (C_{15}, C_{16}, C_{17}). Calculated $R_{O/F}$ and $R_{A/F}$ values for fatty acids were consistently below 1

366   (Figs. 3-5), indicating that these compounds are less abundant in the oven-dried and air-

367 dried samples relative to the freeze-dried samples. The $R_{O/F}$ values were generally lower

368 than the $R_{A/F}$ values for the same compounds, especially among the straight-chain and

369 branched saturated fatty acids (Figs. 3c, 5a-b). Calculated $R_{O/F}$ and $R_{A/F}$ values among

370 saturated straight-chain fatty acids correlate positively with the carbon chain length of the

371 compound ($p<0.05$) (Fig. 3a, b). The correlation between $R_{A/F}$ and chain length is

372 stronger (Fig. 3b) than the correlation between $R_{O/F}$ and chain length (Fig. 3a), which is

373 reflected in a steeper slope of the best linear fit and a higher R^2 value. Relatedly, $R_{A/F}$ and

374 $R_{O/F}$ values are similar at lower molecular weights and diverge at higher molecular

375 weights, with $R_{A/F}$ values consistently higher (closer to a value of 1) than $R_{O/F}$ values.

376 The greater overall depression in fatty acid abundances as a result of oven-drying

377 suggests that physical mechanisms like volatilization, which depends upon chain length

378 and molar mass, play an important role in the effects of drying treatment on straight-

379 chain saturated fatty acid abundances (Meylan and Howard 1991; Lide 1996; Daubert

380 1997; Schwarzenbach et al. 2003). Thus, drying temperatures can influence the

381 distribution of fatty acids in a sample by driving differential loss of compounds with

382 varying molecular weights and volatility.

383   There is no clear relationship between chain length and $R_{O/F}$ and $R_{A/F}$ values for

384 unsaturated straight-chain and saturated branched fatty acids quantified across samples,

385 as they are relatively invariant and below 1 across chain lengths (Figs. 4, 5). Among the

386 straight-chain unsaturated fatty acids, ratios tend to decrease with increasing numbers of

387 non-single bonds, indicating that compounds with higher degrees of unsaturation are less

388 physically stable and therefore more sensitive to the effects of air-drying and oven-drying

389 (Lide 1996; Schwarzenbach et al. 2003).

390 Specific alcohols and sterols were identified using a suite of seven standard

391 compounds with different molar masses, carbon chain lengths and environmental origins

392 (Table 3). Calculated $R_{O/F}$ values across blank-corrected samples were lowest (0.57) for

393 gorgosterol, as high as 1.3 for 1-hexadecanol, and averaged at 0.97 ± 0.22 across all

394 compounds (Table 3, Fig. 6a). Calculated $R_{A/F}$ values were 0.86 ± 0.09 (mean $\pm$ 1 S.D.),

395 lowest for gorgosterol (0.68), and highest for 5α-cholestan-3β-ol (0.97) (Fig. 6b).

396 Compared to fatty acid abundances, peak areas of seven sterols and alcohols quantified

397 across the combined particle samples shifted less as a result of different drying

398 treatments. $R_{O/F}$ and $R_{A/F}$ values for all compounds except gorgosterol ranged from 0.83

399 to 1.3 (Fig. 6a-b). These diminished effects may, in part, result from lower vapor

400 pressures associated with sterol compounds relative to fatty acids (Meylan and Howard

401 1991). Only abundances of gorgosterol in the oven-dried and air-dried samples were

402 anomalously depressed (<0.7), while the abundance of 1-hexadecanol in the oven-dried

403 sample was anomalously elevated (>1.25).

404 The anomalously high 1-hexadecanol ratio in the oven-dried combined particle

405 sample may be an artifact of uneven blank subtractions across drying treatments, a

406 proportionally greater subtraction in the freeze-dried sample than in the oven-dried

407 sample (Table S1). In general, blank corrections for other compounds that are similarly

408 abundant in the deployment blank relative to the particle samples could bias the results

409 presented here. Fortunately, lipid abundance comparisons without a blank subtraction do

410 not greatly differ from and in some cases strengthen interpretations based on an initial

411 blank subtraction (Fig. 6). For example, $R_{O/F}$ and $R_{A/F}$ values for sterols/alcohols

412 including 1-hexadecanol prior to blank correction are much closer to 1.0 and much less

413   variable across molecular weights (Fig. 6d-e), strengthening the argument that different

414   drying treatments affect alcohol and sterol abundances less than they affect fatty acid

415   abundances.

416   Overall, the fact that oven-drying and air-drying shift specific lipid abundances

417   according to their physical properties (e.g., molecular weight and structure), while bulk

418   characteristics and thermal stability remain unaffected across treatments, supports the

419   argument that sample treatment effects are abiotic rather than mediated by biological

420   activity. These drying processes may impose enough heat or airflow to physically remove

421   some of the light-weight, more volatile molecules. Further, we argue that effects from

422   two other processes that shift the abundance distributions of lipids in field samples,

423   bacterial degradation (Wakeham and Volkman 1991; Ohman 1996; Wakeham et al.

424   2002) and abiotic oxidation (Wang et al. 2017), are unlikely here. The relatively

425   depressed branched fatty acid abundances, which derive from bacteria, in the oven-dried

426   and air-dried samples (Fig. 5) indicate that the drying period (<24 hours) for the oven-

427   dried and air-dried samples was likely short enough to limit any significant alteration by

428   heterotrophic activity. Further, Wang et al. (2017) observed that oxidative breakdown of

429   higher chain-length *n*-alkanes at temperatures as low as 60°C generated lower chain-

430   length *n*-alkane by-products, shifting the lipid distribution in soils collected from the

431   field. Our lipid data set does not support this process, exhibiting the reverse relationship

432   between chain length and straight-chain saturated fatty acid abundances and no

433   relationship between chain length and straight-chain unsaturated/branched saturated fatty

434   acid abundances.

435

4   Discussion

The bulk and ramped oxidation analyses of particle samples suggest that preservation of marine POC from the field by oven and air-drying does not compromise the bulk isotope composition, bulk C/N and thermal stability of the sample compared to storage at -80°C and freeze-drying. Thus, samples dried quickly, i.e., in less than 24 hours, at temperatures between 25°C and 56°C, can still be characterized by these metrics. By contrast, filter-normalized and blank-corrected abundances of extracted lipids across POC samples show that oven-drying and air-drying do shift lipid abundances, and that the magnitude of this shift depends on compound structure and molecular size. These results generally agree with prior research demonstrating that warmer sample storage temperatures differentially compromise distinct lipid classes (Ohman 1996). But, this study expands our understanding of temperature effects on POC sample preservation by directly investigating the impact of different drying temperatures rather than different storage temperatures. Unlike earlier studies, this assessment shows that the differences in lipid composition among drying treatments over shorter time scales of less than one day derive from abiotic processes like compound volatilization, rather than biotic processes like enzymatic or heterotrophic degradation, which may be more important when considering wet storage of samples above -80°C.

Typically, lipids make up at most 25% of total biomass in living microalgae (Finkel et al. 2016), which are the primary producers of POC in the shallow, coastal waters of Woods Hole in June. In this study, we have monitored only a small fraction of the marine lipid pool (Wakeham and Volkman 1991), and have found that some

20

459   compounds are as much as ~90% depleted in non-freeze-dried samples relative to freeze-

460   dried samples. More than 50% of several of these compounds, however, are still present

461   in oven-dried and air-dried sample POC relative to freeze-dried POC. Taken together,

462   such shifts in compound-specific abundances as a result of different drying treatments

463   must be small relative to the bulk organic matter composition, as bulk $\delta^{13}C$, $\delta^{15}N$, C/N

464   and thermal stability do not vary across drying treatments.

465

466   **5   Comments and recommendations**

467

468   The results of this sample treatment comparison highlight several characteristics

469   of POC composition (bulk C/N, $\delta^{13}C$, $\delta^{15}N$, and thermal stability) that are not

470   compromised by oven-drying at 56°C or air-drying at high flow and room temperature

471   when the particle samples are dried within 24 hours following collection. As this

472   approach to sample treatment is common in the field (e.g., Buesseler et al. 2005; Bishop

473   and Wood 2008; Bishop et al. 2012; Lam et al. 2015; Rosengard et al. 2015), these

474   findings imply that a vast repository of marine particle samples collected at sea remain

475   useful tracers of POC composition and cycling in the water column, even if originally

476   unintended for such research questions at the time of collection. These particle samples

477   collected and processed by such drying treatments may still be used for bulk organic

478   analysis and ramped pyrolysis/oxidation, the latter of which will expand the empirical

479   applications of this method to understanding marine POC dynamics in the water column.

480   At the same time, these samples are not appropriate for lipid analysis. Oven-

481   drying and air-drying do shift the lipid distribution and potentially the distribution of

21

482   other compound classes in organic matter. The magnitude of these effects on compound

483   class abundances are overwhelmed by a greater proportion of unaltered material in the

484   bulk carbon pool. The data here do not shed light on how the compound-specific stable

485   carbon isotope composition of these compound classes may be altered by oven-drying or

486   air-drying, i.e., whether there is a fractionation effect associated with molecular

487   volatilization of compounds off of QMA filters during the drying process (Wang et al.

488   2017). Furthermore, this report does not suggest that slower flow air-drying at room

489   temperature, rather than higher flow air, would similarly conserve the bulk and thermal

490   stability properties of POC. These uncertainties would be appropriate for future studies

491   with a comparably controlled approach.

492

493

494 **References**

495

496　Bishop, J. K., P. J. Lam, and T. J. Wood. 2012. Getting good particles: Accurate
497　　　　sampling of particles by large volume in-situ filtration. Limnol. Oceanogr.
498　　　　Methods **10:** 681-710.
499　Bishop, J. K. B., and T. J. Wood. 2008. Particulate matter chemistry and dynamics in the
500　　　　twilight zone at VERTIGO ALOHA and K2 sites. Deep Sea Research Part I:
501　　　　Oceanographic Research Papers **55:** 1684-1706.
502　Buesseler, K. O., J. E. Andrews, S. M. Pike, M. A. Charette, L. E. Goldson, M. A.
503　　　　Brzezinski, and V. P. Lance. 2005. Particle export during the southern ocean iron
504　　　　experiment (SOFeX). Limnology and Oceanography **50:** 311-327.
505　Burd, A. B., S. Frey, A. Cabre, and others. 2016. Terrestrial and marine perspectives on
506　　　　modeling organic matter degradation pathways. Global Change Biology **22:** 121-
507　　　　136.
508　Burdige, D. J. 2007. Preservation of Organic Matter in Marine Sediments: Controls,
509　　　　Mechanisms, and an Imbalance in Sediment Organic Carbon Budgets? Chemical
510　　　　Reviews **107:** 467-485.
511　Cavagna, A.-J., F. Dehairs, S. Bouillon, V. Woule-Ebongué, F. Planchon, B. Delille, I.
512　　　　Bouloubassi. 2013. Water column distribution and carbon isotopic signal of
513　　　　cholesterol, brassicasterol and particulate organic carbon in the Atlantic sector of
514　　　　the Southern Ocean. Biogeosciences **10:** 2787-2801.
515　Cramer, B. 2004. Methane generation from coal during open system pyrolysis
516　　　　investigated by isotope specific, Gaussian distributed reaction kinetics. Organic
517　　　　Geochemistry **35:** 379-392.
518　Daubert, T. 1997. Physical and thermodynamic properties of pure chemicals, National
519　　　　Standard Reference Data System. American Institute of Chemical Engineering.
520　Finkel, Z. V., M. J. Follows, J. D. Liefer, C. M. Brown, I. Benner, and A. J. Irwin. 2016.
521　　　　Phylogenetic Diversity in the Macromolecular Composition of Microalgae. PloS
522　　　　one **11**.
523　Francois, R., S. Honjo, R. Krishfield, and S. Manganini. 2002. Factors controlling the
524　　　　flux of organic carbon to the bathypelagic zone of the ocean. Global
525　　　　Biogeochemical Cycles **16:** doi:10.1029/2001GB001722.
526　Grimalt, J. O., E. Torras, and J. Albaigés. 1988. Bacterial reworking of sedimentary lipids
527　　　　during sample storage. Organic Geochemistry **13:** 741-746.
528　Hemingway, J. D., V. V. Galy, A. R. Gagnon, K. E. Grant, S. Z. Rosengard, G. Soulet, P.
529　　　　K. Zigah, and A. P. McNichol. 2017. Assessing the Blank Carbon Contribution,
530　　　　Isotope Mass Balance, and Kinetic Isotope Fractionation of the Ramped
531　　　　Pyrolysis/Oxidation Instrument at NOSAMS. Radiocarbon **59:** 179-193.
532　Kaehler, S., and E. Pakhomov. 2001. Effects of storage and preservation on the d13C and
533　　　　d15N signatures of selected marine organisms. Marine Ecology Progress Series
534　　　　**219:** 299-304.
535　Lam, P. J., D. C. Ohnemus, and M. E. Auro. 2015. Size-fractionated major particle
536　　　　composition and concentrations from the US GEOTRACES north Atlantic zonal

537   transect. Deep Sea Research Part II: Topical Studies in Oceanography **116:** 303-
538   320.
539 Lide, D. R. 1996. Handbook of Chemistry and Physics: CRC Handbook. CRC Press.
540 Meylan, W. M., and P. H. Howard. 1991. Bond contribution method for estimating
541   Henry's law constants. Environmental toxicology and chemistry **10:** 1283-1293.
542 Ohman, M. 1996. Freezing and storage of copepod samples for the analysis of lipids.
543   Marine ecology progress series **130:** 295-298.
544 Repeta, D. J. 2014. Chemical characterization and cycling of dissolved organic matter, p.
545   21–63. In D. A. Hansell and C. A. Carlson [eds.], Biogeochemistry of marine
546   dissolved organic matter. Elsevier.
547 Rosengard, S. Z., P. J. Lam, W. M. Balch, M. E. Auro, S. Pike, D. Drapeau, and B.
548   Bowler. 2015. Carbon export and transfer to depth across the Southern Ocean
549   Great Calcite Belt. Biogeosciences **12:** 3953-3971.
550 Rosenheim, B. E., M. B. Day, E. Domack, H. Schrum, A. Benthien, and J. M. Hayes.
551   2008. Antarctic sediment chronology by programmed-temperature pyrolysis:
552   Methodology and data treatment. Geochem. Geophys. Geosyst. **9**: Q04005.
553   doi:10.1029/2007GC001816
554 Rosenheim, B. E., and V. Galy. 2012. Direct measurement of riverine particulate organic
555   carbon age structure. Geophys. Res. Lett. **39**: L19703.
556   doi:10.1029/2012GL052883
557 Rosenheim, B. E., K. M. Roe, B. J. Roberts, A. S. Kolker, M. A. Allison, and K. H.
558   Johannesson. 2013. River discharge influences on particulate organic carbon age
559   structure in the Mississippi/Atchafalaya River System. Global Biogeochem.
560   Cycles **27**: 154–166. doi:10.1002/gbc.20018
561 Schwarzenbach, R. P., P. M. Gschwend, and D. M. Imboden. 2003. Environmental
562   organic chemistry. John Wiley & Sons.
563 Subt, C., K. A. Fangman, J. S. Wellner, and B. E. Rosenheim. 2016. Sediment
564   chronology in Antarctic deglacial sediments: Reconciling organic carbon 14C
565   ages to carbonate 14C ages using Ramped PyrOx. The Holocene **26:** 265-273.
566 Trull, T., and L. Armand. 2001. Insights into Southern Ocean carbon export from the
567   δ^{13}C of particles and dissolved inorganic carbon during the SOIREE iron release
568   experiment. Deep Sea Research Part II: Topical Studies in Oceanography **48:**
569   2655-2680.
570 Wagner, B. A., G. R. Buettner, and C. P. Burns. 1994. Free Radical-Mediated Lipid
571   Peroxidation in Cells: Oxidizability Is a Function of Cell Lipid bis-Allylic
572   Hydrogen Content. Biochemistry **33:** 4449-4453.
573 Wakeham, S. G., and E. A. Canuel. 1988. Organic geochemistry of particulate matter in
574   the eastern tropical North Pacific Ocean: Implications for particle dynamics.
575   Journal of Marine Research **46:** 183-213.
576 Wakeham, S. G., M. L. Peterson, J. I. Hedges, and C. Lee. 2002. Lipid biomarker fluxes
577   in the Arabian Sea, with a comparison to the equatorial Pacific Ocean. Deep-Sea
578   Research Part Ii-Topical Studies in Oceanography **49:** 2265-2301.
579 Wakeham, S. G., and J. K. Volkman. 1991. Sampling and analysis of lipids in marine
580   particulate matter, p. 171–179. In D. C. Hurd and D. W. Spencer [eds.], Marine
581   particles: Analysis and characterization. American Geophysical Union.
582 Wang, C., Y. Eley, A. Oakes, and M. Hren. 2017. Hydrogen isotope and molecular

583   alteration of n-alkanes during heating in open and closed systems. Org. Geochem.
584   112: 47–58. doi:10.1016/j.orggeochem.2017.07.006

585 Table 1. The bulk composition of <51 µm particulate organic matter loaded onto three sample and two blank <51 µm QMA filters

586 (active area ~ 125 cm^2) that were either dried in an oven, laminar flow hood or freeze-dried. Filters were divided into thirds prior to

587 drying so that each treatment could be applied to each blank or sample filter. Sub-samples from individual thirds of different McLane

588 pump deployments were analyzed for bulk composition. Particle sample values here were not blank-corrected.

589

Sample	Deployment	Volume (L)	Treatment	C/*filter**	[C]*	[N]*	C/N	$\delta^{13}C$	$\delta^{15}N$
--	--	*L*	--	*mg/filter*	*µM*	*µM*	*µmol/µmol*	*‰*	*‰*
POC1	1	95.4	oven-dried						
POC1	1	95.4	air-dried	14	12.4	1.9	6.5	-23.6	7.9
POC1	1	95.4	freeze-dried						
POC2	1	93.8	oven-dried						
POC2	1	93.8	air-dried						
POC2	1	93.8	freeze-dried	13	11.9	1.8	6.8	-23.9	8.3
POC3	2	40.5	oven-dried	8	16.7	2.5	6.8	-23.8	8.2
POC3	2	40.5	air-dried						
POC3	2	40.5	freeze-dried						
db1	1	0	oven-dried						
db1	1	0	air-dried						
db1	1	0	freeze-dried	0.7	N/A	N/A	7.7	-25.6	BDL
db2	2	0	oven-dried						
db2	2	0	air-dried						
db2	2	0	freeze-dried						

590 BDL= below detection limit.
591 "db"= deployment blank.
592 *quantities are normalized to active area of the QMA filter, 125 cm^2
593

26

594 Table 2. Carbon released per analysis and filter-normalized carbon yields calculated from

595 ramped oxidation of sample and deployment blank filters. No CO_2 quantities were

596 measured and converted to carbon mass during the second freeze-dried sample analysis.

597 Carbon values reported here were not blank-corrected.

598

| Sample Type	Treatment	Analysis #	Oven	mg C/analysis	Fraction of OMA analyzed	mg C/filter (125 cm^2)	
POC1+2+3	Oven-dried	I	A	0.697	5%	12.8	
POC1+2+3	Oven-dried	II	A	0.337	3%	12.4	**Mean ± S.D.**
POC1+2+3	Oven-dried	III	B	0.346	3%	12.7	12.6 ± 0.2
POC1+2+3	Air-dried	I	A	0.678	5%	12.5	
POC1+2+3	Air-dried	II	B	0.352	3%	12.9	**Mean ± S.D.**
POC1+2+3	Air-dried	III	B	0.286	3%	10.5	12.0 ± 1.3
POC1+2+3	Freeze-dried	I	A	0.721	5%	13.2	
POC1+2+3	Freeze-dried	II	B	no data	3%	no data	
POC1+2+3	Freeze-dried	III	B	0.314	3%	11.5	
db1+2	Oven-dried	I	A	0.050	9%	0.5	
db1+2	Air-dried	I	A	0.042	9%	0.5	**Mean ± S.D.**
db1+2	Freeze-dried	I	A	0.104	9%	1.1	0.7 ± 0.4

599   "db"=deployment blank

600   Table 3. Constituents of the alcohol/sterol standards and their properties.

601

Standard compound	Class	Molar Mass	# Carbon	Known sources
--	--	*g/mol*	*#*	--
Phytol	Alcohol	196.539	20	Chlorophyll
1-hexadecanol	Alcohol	242.447	16	Ubiquitous
Cholesterol	Sterol	386.664	27	Ubiquitous
5α-cholestan-3β-ol	Sterol	388.68	27	Cholesterol derivative in biological matter
Brassicasterol	Sterol	398.675	28	Unicellular algae, some terrestrial plants
Stigmasterol	Sterol	412.702	29	Terrestrial vegetation
Gorgosterol	Sterol	426.729	30	Marine algae

602
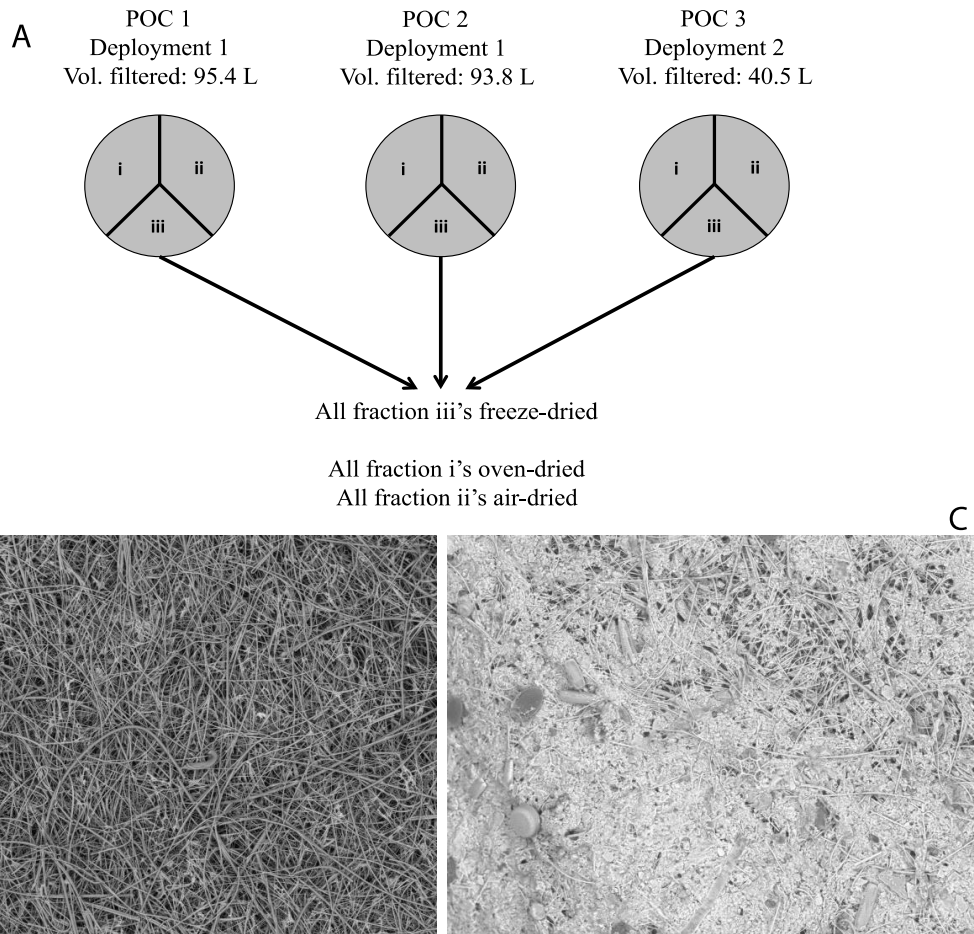
Figure 1. (a) Schematic of dock sample collection and post-processing before analysis. A similar approach was used to apportion the two deployment blank filters by drying tr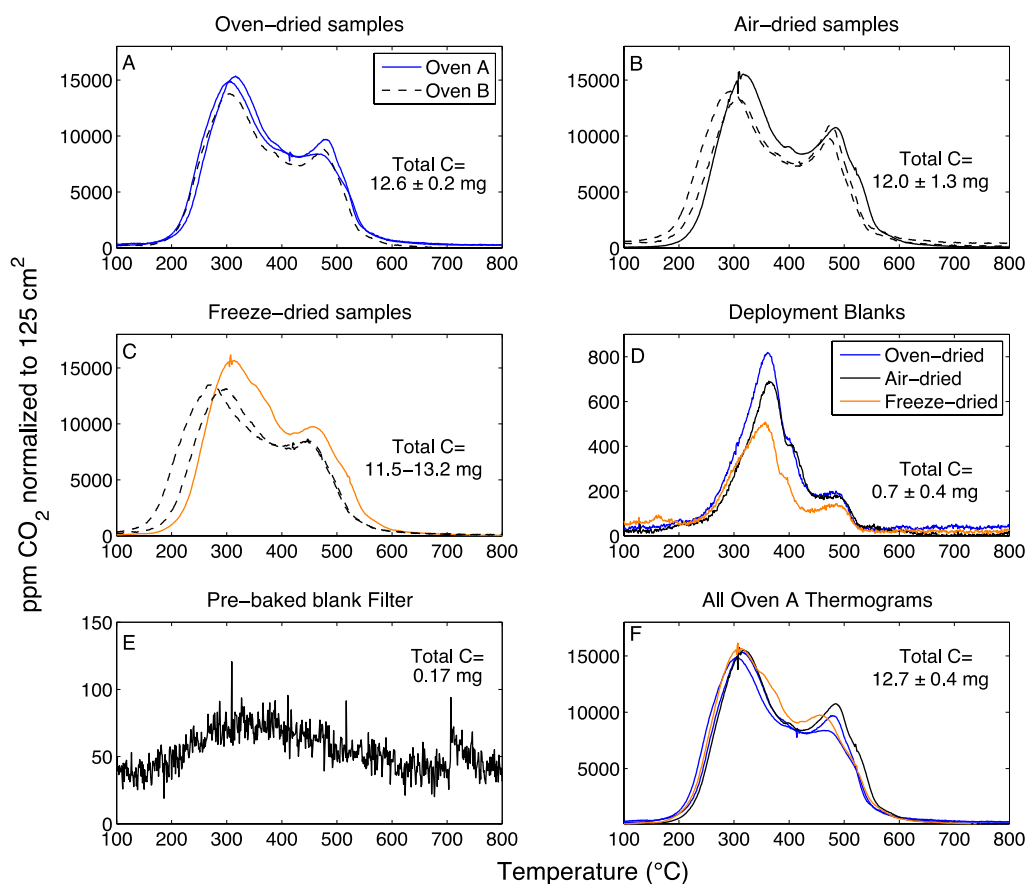eatment. (b-c) Scanning electron microscope images of freeze-dried (b) deployment blank and (c) sample particle filters. The images in b-c are ~0.6 cm wide. Total filter active area is 125cm^2, corresponding to a ~12.6 cm diameter.

611
612 Figure 2. (a-c) Thermograms of combined particle sample filters generated by ramped

613 oxidation, with replicate analyses plotted as solid colored lines (either blue, black or

614 orange) when using furnace A vs. black dashed lines when using oven B. (d)

615 Thermograms of deployment blanks, analyzed once per drying treatment in oven A. (e)

616 Thermogram of a pre-combusted non-deployed QMA filter, also analyzed using oven A.

617 (f) All sample particle thermograms analyzed in oven A. The legend in (d) applies to (f).

618

619
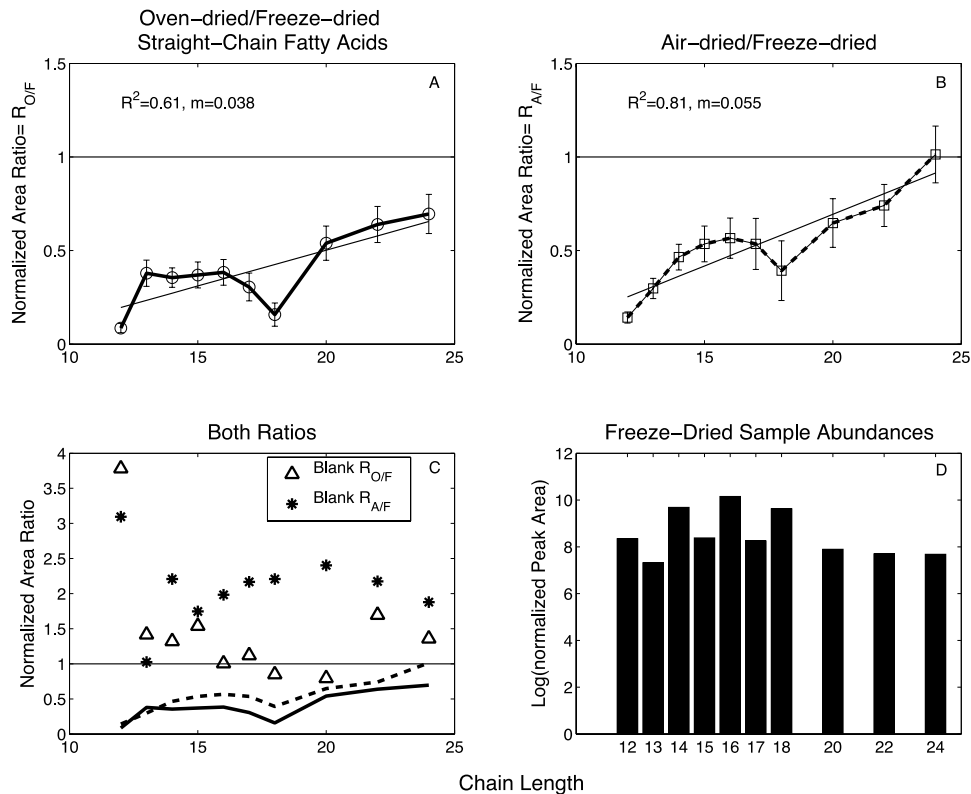
Figure 3. (a-c) Ratios of filter-normalized and blank-corrected peak areas of straight-chain saturated fatty acids in (a) oven-dried particle samples relative to freeze-dried samples ($R_{O/F}$) and in (b) air-dried samples relative to freeze-dried samples ($R_{A/F}$). These ratios correlate significantly with compound carbon chain length (p<0.05). R^2 and the slope (*m*) values of each correlation are reported. Errors for each ratio were calculated by propagating errors for filter-normalized peak abundances (~10%). (c) $R_{O/F}$ and $R_{A/F}$ plotted on the same axes, along with ratios of oven-dried (triangle) or air-dried (star) blank compound abundances to freeze-dried blank compound abundances. The relative errors of these ratios in the deployment blanks are <1% and thus not shown. (d) Absolute normalized and blank-corrected peak areas in the freeze-dried samples.

31

632   Figure 4.
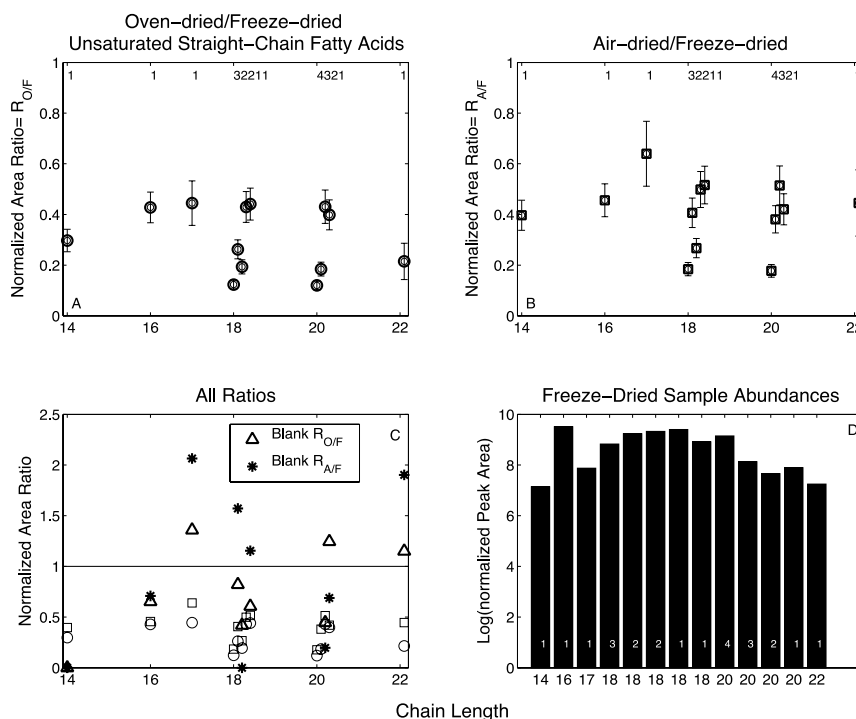
633   (a-b) Ratios of filter-normalized and blank-corrected peak areas of straight-chain

634   unsaturated fatty acids in (a) oven-dried particle samples relative to freeze-dried samples

635   ($R_{O/F}$) and in (b) air-dried samples relative to freeze-dried samples ($R_{A/F}$). Errors for each

636   ratio were calculated by propagating errors for filter-normalized peak abundances

637   (~10%). The numbers on the panels indicate the degrees of unsaturation, or number of

638   non-single bonds, for compounds plotted that have the same carbon chain length. For

639   example, the cluster of four data points around chain length 20 refers to a 20-carbon fatty

640   acid with one to four non-single bonds. (c) $R_{O/F}$ and $R_{A/F}$ plotted on the same axes

641   alongside ratios of oven-dried (triangle) or air-dried (star) blank compound abundances to

642   freeze-dried blank compound abundances. The relative errors of these ratios in the

643   deployment blanks are <1% and are thus not shown. (d) Absolute normalized and blank-

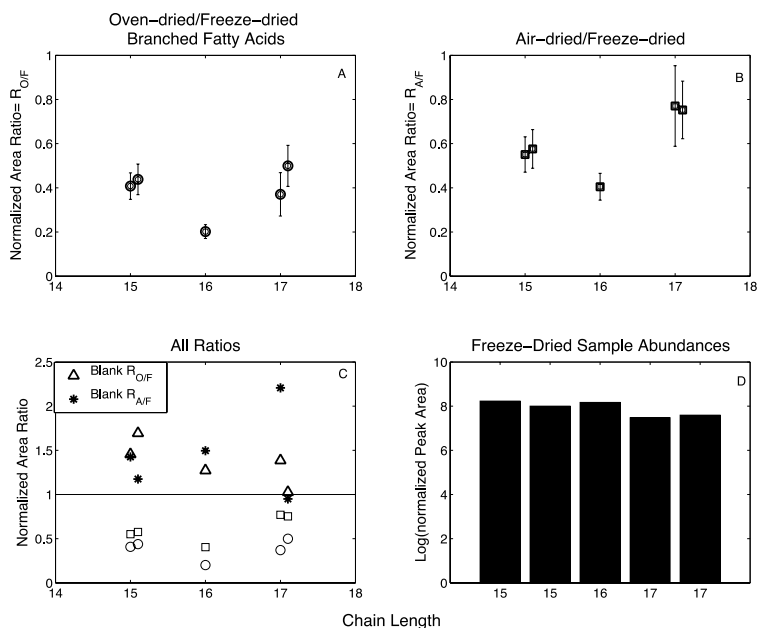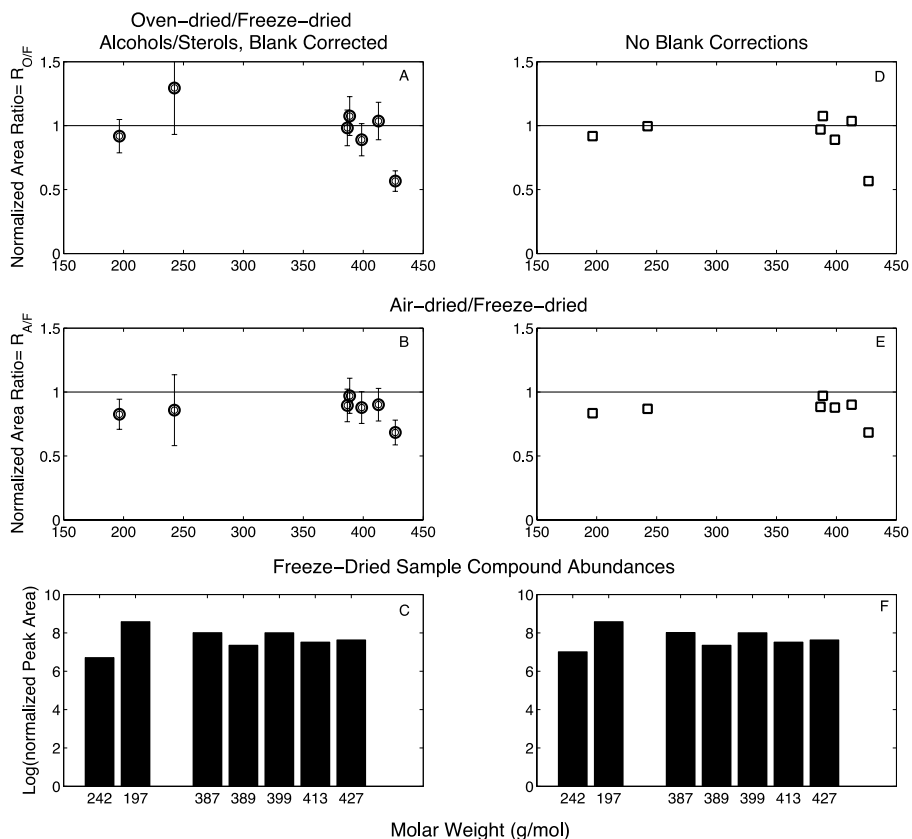644   corrected peak areas in the freeze-dried samples ordered by chain length. The bars are

645   labeled by the number of non-single bonds in the compound plotted.

32

646

647 Figure 5. (a-b) Ratios of filter-normalized and blank-corrected peak areas of three

648 branched saturated fatty acids in (a) oven-dried particle samples relative to freeze-dried

649 samples ($R_{O/F}$) and in (b) air-dried samples relative to freeze-dried samples ($R_{A/F}$). Errors

650 for each ratio were calculated by propagating errors for filter-normalized peak

651 abundances (~10%). The two clusters of data points at chain lengths 15 and 17 represent

652 isomers of the same size molecule. The pair of 15 chain length compounds corresponds

653 to the iso- and anteiso-methyl-branched fatty acids from left to right, respectively. The

654 leftmost data point of the 17 chain length pair corresponds to the iso-methyl-branched

655 fatty acid, while the rightmost data point corresponds to the heterocyclic isomer cis-9,10-

656 methylenehexadecanoate. (c) $R_{O/F}$ and $R_{A/F}$ plotted on the same axes alongside ratios of

657 oven-dried (triangle) or air-dried (star) blank compound abundances to freeze-dried blank

658 compound abundances. The relative errors of these ratios in the deployment blanks are

659 <1% and are thus not shown. (d) Absolute normalized and blank-corrected peak areas in

660 the freeze-dried samples.

33

661

Figure 6. (a-b) Ratios of filter-normalized and blank-corrected peak areas of seven

alcohols/sterols in (a) oven-dried particle samples relative to freeze-dried samples ($R_{O/F}$)

and in (b) air-dried samples relative to freeze-dried samples ($R_{A/F}$). Errors for each ratio

were calculated by propagating errors for filter-normalized peak abundances (~10%). The

x-axis is molar weight, which matches the compounds listed in Table 3. (c) Absolute

normalized blank-corrected peak areas of alcohols/sterols in the freeze-dried sample.

Quantities in panels d-f are analogous to quantities in a-c, but are not blank-corrected.

Relative errors for ratios in d-e, not plotted, are <1%.

670
671

34

Table S1. Abundances of select fatty acids, alcohols and sterols quantified in freeze-dried, air-dried and oven-dried particle samples (POC1+2+3) and deployment blanks (db1+2). The abundances are represented as peak areas normalized to the total active area of a QMA filter, 125 cm^2, but are not blank-corrected. "Fraction from blank" is the abundance of each compound in the freeze-dried, oven-dried or air-dried sample deployment blank filters relative to the abundance observed in the freeze-dried, oven-dried or air-dried particle sample filters, respectively. The $R_{O/F}$ and $R_{A/F}$ values are ratios of either oven-dried or air-dried compound peak areas to freeze-dried compound peak areas in the blank filters or in the particle samples prior to blank subtraction. Note that these ratios differ in samples and blanks, which justifies the choice to subtract blank contributions from sample peak abundances before calculating the ratios presented in Section 3.3. The straight-chain fatty acids are named as C followed by chain length: number of double bonds. The branched fatty acids are named with a "C" followed by just the chain length.

Sample or blank	Treatment	Compound	Normalized Peak Area	Fraction from blank	$R_{O/F}$ or $R_{A/F}$
--	--	--		%	--
POC1+2+3	Freeze	C12:0	230,730,000	3%	
POC1+2+3	Freeze	C13:0	23,175,000	10%	
POC1+2+3	Freeze	C14:1	15,356,000	10%	
POC1+2+3	Freeze	C14:0	4,934,400,000	1%	
POC1+2+3	Freeze	C15, branched[a]	172,350,000	2%	
POC1+2+3	Freeze	C15, branched[b]	104,040,000	4%	
POC1+2+3	Freeze	C15:0	265,890,000	10%	
POC1+2+3	Freeze	C16, branched	151,780,000	2%	
POC1+2+3	Freeze	C16:1	3,254,100,000	0.2%	
POC1+2+3	Freeze	C16:0	16,057,000,000	11%	
POC1+2+3	Freeze	C17, branched[a]	38,213,000	22%	
POC1+2+3	Freeze	C17:1	87,019,000	14%	

POC1+2+3	Freeze	C17, branched[c]	46,106,000	16%	
POC1+2+3	Freeze	C17:0	222,260,000	20%	
POC1+2+3	Freeze	C18:3	674,290,000	0%	
POC1+2+3	Freeze	C18:2[d]	1,729,500,000	0.5%	
POC1+2+3	Freeze	C18:2[e]	2,137,900,000	1%	
POC1+2+3	Freeze	C18:1[f]	2,524,800,000	0%	
POC1+2+3	Freeze	C18:1[g]	829,260,000	1%	
POC1+2+3	Freeze	C18:0	5,869,600,000	28%	
POC1+2+3	Freeze	C20:4	1,408,700,000	0%	
POC1+2+3	Freeze	C20:3	135,710,000	0%	
POC1+2+3	Freeze	C20:2	49,256,000	7%	
POC1+2+3	Freeze	C20:1	81,094,000	2%	
POC1+2+3	Freeze	C20:0	91,031,000	13%	
POC1+2+3	Freeze	C22:1	22,969,000	23%	
POC1+2+3	Freeze	C22:0	52,069,000	3%	
POC1+2+3	Freeze	C24:0	49,969,000	4%	
POC1+2+3	Freeze	1-hexadecanol	10,306,000	51%	
POC1+2+3	Freeze	Phytol	385,380,000	0.4%	
POC1+2+3	Freeze	Cholesterol	104,050,000	1%	
POC1+2+3	Freeze	5α-cholestan-3-β-ol	22,578,000	0%	
POC1+2+3	Freeze	Brassicasterol	100,870,000	0%	
POC1+2+3	Freeze	Stigmasterol	33,172,000	0%	
POC1+2+3	Freeze	Gorgosterol	42,698,000	0%	
POC1+2+3	Oven	C12:0	45,326,000	58%	0.20
POC1+2+3	Oven	C13:0	11,176,000	29%	0.48
POC1+2+3	Oven	C14:1	4,112,900	0%	0.27
POC1+2+3	Oven	C14:0	1,824,200,000	5%	0.37
POC1+2+3	Oven	C15, branched[a]	73,059,000	5%	0.42
POC1+2+3	Oven	C15, branched[b]	51,341,000	15%	0.49
POC1+2+3	Oven	C15:0	128,160,000	31%	0.48
POC1+2+3	Oven	C16, branched	34,648,000	14%	0.23
POC1+2+3	Oven	C16:1	1,393,700,000	0.3%	0.43
POC1+2+3	Oven	C16:0	7,295,100,000	25%	0.45
POC1+2+3	Oven	C17, branched[a]	22,645,000	51%	0.59
POC1+2+3	Oven	C17:1	49,980,000	34%	0.57
POC1+2+3	Oven	C17, branched[c]	26,804,000	27%	0.58
POC1+2+3	Oven	C17:0	103,250,000	47%	0.46
POC1+2+3	Oven	C18:3	83,036,000	0%	0.12
POC1+2+3	Oven	C18:2[d]	458,330,000	2%	0.27
POC1+2+3	Oven	C18:2[e]	419,150,000	3%	0.20
POC1+2+3	Oven	C18:1[f]	1,084,600,000	0%	0.43
POC1+2+3	Oven	C18:1[g]	366,900,000	1%	0.44
POC1+2+3	Oven	C18:0	2,045,600,000	67%	0.35

POC1+2+3	Oven	C20:4	168,990,000	0%	0.12
POC1+2+3	Oven	C20:3	27,352,000	9%	0.20
POC1+2+3	Oven	C20:2	21,258,000	7%	0.43
POC1+2+3	Oven	C20:1	33,895,000	7%	0.42
POC1+2+3	Oven	C20:0	52,092,000	18%	0.57
POC1+2+3	Oven	C22:1	9,888,500	62%	0.43
POC1+2+3	Oven	C22:0	35,163,000	9%	0.68
POC1+2+3	Oven	C24:0	36,053,000	7%	0.72
POC1+2+3	Oven	1-hexadecanol	10,266,000	36%	1.00
POC1+2+3	Oven	Phytol	353,840,000	0.4%	0.92
POC1+2+3	Oven	Cholesterol	100,910,000	0%	0.97
POC1+2+3	Oven	5α-cholestan-3-β-ol	24,272,000	0%	1.08
POC1+2+3	Oven	Brassicasterol	89,803,000	0%	0.89
POC1+2+3	Oven	Stigmasterol	34,373,000	0%	1.04
POC1+2+3	Oven	Gorgosterol	24,195,000	0%	0.57
POC1+2+3	Air	C12:0	53,204,000	40%	0.23
POC1+2+3	Air	C13:0	8,572,600	28%	0.37
POC1+2+3	Air	C14:1	5,493,400	0%	0.36
POC1+2+3	Air	C14:0	2,421,700,000	7%	0.49
POC1+2+3	Air	C15, branched[a]	97,270,000	4%	0.56
POC1+2+3	Air	C15, branched[b]	62,692,000	9%	0.60
POC1+2+3	Air	C15:0	173,380,000	26%	0.65
POC1+2+3	Air	C16, branched	65,582,000	9%	0.43
POC1+2+3	Air	C16:1	1,485,300,000	0.3%	0.46
POC1+2+3	Air	C16:0	11,687,000,000	31%	0.73
POC1+2+3	Air	C17, branched[a]	41,455,000	45%	1.08
POC1+2+3	Air	C17:1	73,241,000	35%	0.84
POC1+2+3	Air	C17, branched[c]	36,104,000	19%	0.78
POC1+2+3	Air	C17:0	189,910,000	50%	0.85
POC1+2+3	Air	C18:3	124,130,000	0%	0.18
POC1+2+3	Air	C18:2[d]	713,190,000	2%	0.41
POC1+2+3	Air	C18:2[e]	564,150,000	0%	0.26
POC1+2+3	Air	C18:1[f]	1,280,800,000	2%	0.51
POC1+2+3	Air	C18:1[g]	433,400,000	2%	0.52
POC1+2+3	Air	C18:0	5,243,000,000	68%	0.89
POC1+2+3	Air	C20:4	249,840,000	0%	0.18
POC1+2+3	Air	C20:3	51,672,000	0%	0.38
POC1+2+3	Air	C20:2	24,210,000	3%	0.49
POC1+2+3	Air	C20:1	34,600,000	4%	0.43
POC1+2+3	Air	C20:0	79,482,000	35%	0.87
POC1+2+3	Air	C22:1	17,952,000	56%	0.78
POC1+2+3	Air	C22:0	41,130,000	9%	0.79
POC1+2+3	Air	C24:0	52,335,000	7%	1.05

POC1+2+3	Air	1-hexadecanol	8,954,100	51%	0.87
POC1+2+3	Air	Phytol	321,560,000	1%	0.83
POC1+2+3	Air	Cholesterol	91,996,000	0%	0.88
POC1+2+3	Air	5α-cholestan-3-β-ol	21,919,000	0%	0.97
POC1+2+3	Air	Brassicasterol	88,627,000	0%	0.88
POC1+2+3	Air	Stigmasterol	29,892,000	0%	0.90
POC1+2+3	Air	Gorgosterol	29,202,000	0%	0.68
db1+2	Freeze	C12:0	6,916,400		
db1+2	Freeze	C13:0	2,308,700		
db1+2	Freeze	C14:1	1,517,400		
db1+2	Freeze	C14:0	73,738,000		
db1+2	Freeze	C15, branched[a]	2,668,500		
db1+2	Freeze	C15, branchedb1+2	4,570,200		
db1+2	Freeze	C15:0	25,625,000		
db1+2	Freeze	C16, branched	3,793,500		
db1+2	Freeze	C16:1	6,860,900		
db1+2	Freeze	C16:0	1,831,900,000		
db1+2	Freeze	C17, branched[a]	8,362,700		
db1+2	Freeze	C17:1	12,346,000		
db1+2	Freeze	C17, branched[c]	7,156,200		
db1+2	Freeze	C17:0	43,444,000		
db1+2	Freeze	C18:3	-		
db1+2	Freeze	C18:2[d]	8,610,200		
db1+2	Freeze	C18:2[e]	25,589,000		
db1+2	Freeze	C18:1[f]	-		
db1+2	Freeze	C18:1[g]	8,262,500		
db1+2	Freeze	C18:0	1,620,100,000		
db1+2	Freeze	C20:4	-		
db1+2	Freeze	C20:3	-		
db1+2	Freeze	C20:2	3,576,000		
db1+2	Freeze	C20:1	1,876,600		
db1+2	Freeze	C20:0	11,724,000		
db1+2	Freeze	C22:1	5,301,600		
db1+2	Freeze	C22:0	1,777,600		
db1+2	Freeze	C24:0	1,956,900		
db1+2	Freeze	1-hexadecanol	5,209,300		
db1+2	Freeze	Phytol	1,421,900		
db1+2	Freeze	Cholesterol	1,341,700		
db1+2	Freeze	5α-cholestan-3-β-ol	-		
db1+2	Freeze	Brassicasterol	-		
db1+2	Freeze	Stigmasterol	-		
db1+2	Freeze	Gorgosterol	-		
db1+2	Oven	C12:0	26,156,000		3.78

db1+2	Oven	C13:0	3,271,000	1.42
db1+2	Oven	C14:1	-	0.00
db1+2	Oven	C14:0	97,448,000	1.32
db1+2	Oven	C15, branched[a]	3,881,200	1.45
db1+2	Oven	C15, branched[b]	7,740,500	1.69
db1+2	Oven	C15:0	39,432,000	1.54
db1+2	Oven	C16, branched	4,827,200	1.27
db1+2	Oven	C16:1	4,476,400	0.65
db1+2	Oven	C16:0	1,842,100,000	1.01
db1+2	Oven	C17, branched[a]	11,587,000	1.39
db1+2	Oven	C17:1	16,773,000	1.36
db1+2	Oven	C17, branched[c]	7,352,200	1.03
db1+2	Oven	C17:0	48,682,000	1.12
db1+2	Oven	C18:3	-	-
db1+2	Oven	C18:2[d]	7,065,000	0.82
db1+2	Oven	C18:2[e]	10,735,000	0.42
db1+2	Oven	C18:1[f]	-	-
db1+2	Oven	C18:1[g]	5,008,500	0.61
db1+2	Oven	C18:0	1,375,200,000	0.85
db1+2	Oven	C20:4	-	-
db1+2	Oven	C20:3	2,349,100	-
db1+2	Oven	C20:2	1,594,100	0.45
db1+2	Oven	C20:1	2,336,500	1.25
db1+2	Oven	C20:0	9,324,700	0.80
db1+2	Oven	C22:1	6,095,700	1.15
db1+2	Oven	C22:0	3,015,400	1.70
db1+2	Oven	C24:0	2,658,700	1.36
db1+2	Oven	1-hexadecanol	3,667,600	0.70
db1+2	Oven	Phytol	1,306,600	0.92
db1+2	Oven	Cholesterol	-	0.00
db1+2	Oven	5α-cholestan-3-β-ol	-	-
db1+2	Oven	Brassicasterol	-	-
db1+2	Oven	Stigmasterol	-	-
db1+2	Oven	Gorgosterol	-	-
db1+2	Air	C12:0	21,406,000	3.09
db1+2	Air	C13:0	2,365,800	1.02
db1+2	Air	C14:1	-	0.00
db1+2	Air	C14:0	162,790,000	2.21
db1+2	Air	C15, branched[a]	3,802,800	1.43
db1+2	Air	C15, branchedb1+2	5,369,700	1.17
db1+2	Air	C15:0	44,762,000	1.75
db1+2	Air	C16, branched	5,673,800	1.50
db1+2	Air	C16:1	4,857,200	0.71

db1+2	Air	C16:0	3,633,300,000	1.98
db1+2	Air	C17, branched[a]	18,454,000	2.21
db1+2	Air	C17:1	25,480,000	2.06
db1+2	Air	C17, branched[c]	6,793,300	0.95
db1+2	Air	C17:0	94,158,000	2.17
db1+2	Air	C18:3	-	-
db1+2	Air	C18:2[d]	13,530,000	1.57
db1+2	Air	C18:2[e]	-	0.00
db1+2	Air	C18:1[f]	22,137,000	-
db1+2	Air	C18:1[g]	9,540,200	1.15
db1+2	Air	C18:0	3,576,200,000	2.21
db1+2	Air	C20:4	-	-
db1+2	Air	C20:3	-	-
db1+2	Air	C20:2	701,330	0.20
db1+2	Air	C20:1	1,291,300	0.69
db1+2	Air	C20:0	28,169,000	2.40
db1+2	Air	C22:1	10,085,000	1.90
db1+2	Air	C22:0	3,865,200	2.17
db1+2	Air	C24:0	3,677,500	1.88
db1+2	Air	1-hexadecanol	4,578,900	0.88
db1+2	Air	Phytol	4,389,300	3.09
db1+2	Air	Cholesterol	-	-
db1+2	Air	5α-cholestan-3-β-ol	-	-
db1+2	Air	Brassicasterol	-	-
db1+2	Air	Stigmasterol	-	-
db1+2	Air	Gorgosterol	-	-

[a]iso
[b]anteiso
[c]cis-9,10-methylenehexadecanoate
[d]cis-9,12-octadecadienoate
[e]trans-9,12-octadecadienoate
[f]cis-9-octadecenoate
[g]trans-9-octadecenoate